Triple Regge exchange and transverse single-spin asymmetries of the very forward neutral pion production in polarized $p+p$ collisions

Hee-Jin Kim,[1,*] Samson Clymton,[1,†] and Hyun-Chul Kim[1,2,‡]

[1]*Department of Physics, Inha University, Incheon 22212, Republic of Korea*
[2]*School of Physics, Korea Institute for Advanced Study (KIAS), Seoul 02455, Republic of Korea*

(Received 8 June 2022; accepted 22 August 2022; published 2 September 2022)

Recently, the RHICf Collaboration measured the transverse single-spin asymmetries of the very forward neutral pion in polarized $p+p$ collisions at $\sqrt{s}=510$ GeV, produced at large pseudorapidity ($\eta \gtrsim 6$). The data show large asymmetries both in longitudinal momentum fraction x_F and transverse momentum p_T at $p_T < 1$ GeV$/c$. Employing baryonic triple Regge exchanges, we describe the complete RHICf data for the first time and show that the neutral pion production at low p_T can be interpreted as a diffractive one.

DOI: 10.1103/PhysRevD.106.054001

I. INTRODUCTION

The spin of the nucleon has been one of the most crucial issues in hadronic physics since the EMC experiment [1]. The nucleon consists of not only three valence quarks but also other partons such as antiquarks and gluons, so the nucleon spin should originate from the partons inside it and their orbital angular momenta [2] together with the contribution of the valence quarks. Thus, one of the most profound questions was addressed: "*How does the spin of the nucleon arise?*" It motivated the future plan for the Electron-Ion Collider (EIC) [3]. Meanwhile, the transverse spin of the nucleon provides yet another aspect to the internal structure of the nucleon. The transverse momentum-dependent functions (TMDs) and the generalized parton distributions (GPDs) furnish the multifaceted aspect of the structure of the polarized nucleon in the transverse plane (see recent reviews [4,5]). Furthermore, sizable transverse single-spin asymmetries (TSSA) of the neutral pion in inclusive pp collisions have been continuously reported well over decades [6–11] (see also recent reviews [5,12]). Since the experimental data from the PHENIX and STAR Collaborations were obtained at higher values of the transverse momentum ($p_T \gtrsim 2$ GeV$/c$) in the midrapidity coverage, where the pseudorapidity is given as $2 < \eta < 4$ [8–11], QCD-based approaches have been employed such as the TMDs [13–15] and collinear twist-3 factorization [16–23] to describe the experimental data. The Jefferson Lab Angular Momentum (JAM) Collaboration [24] has carried out the simultaneous QCD global analysis, considering the data on the TSSA from various high-energy processes.

The TSSA at low transverse momentum in the large pseudorapidity displays the nonperturbative diffractive nature. The RHICf Collaboration measured the TSSA of the neutral pion in transversely polarized $p^{\uparrow}+p$ collision at $\sqrt{s}=510$ GeV and reported that the TSSA increased rapidly as functions of both the longitudinal momentum fraction x_F and low transverse momentum p_T ($p_T < 1$ GeV$/c$) at the pseudorapidity larger than 6 ($\eta > 6$) [25]. The RHICf experiment data posed a question of whether the large values of the TSSA of π^0 are due to diffractive scattering: The values of TSSA rise as p_T increases and reach around 25% at $p_T \simeq 0.8$ GeV$/c$. The dependence on the longitudinal momentum fraction or the Feynman-x variable (x_F) reveals even a drastic feature. In the present work, we will answer for the first time the question addressed by the RHICf Collaboration: Considering the $p^{\uparrow}+p \to \pi^0 + X$ process at low p_T as diffractive scattering and introducing the baryonic triple Regge exchanges, we explain the RHICf data very well.

The current work is organized as follows: In Sec. II, we briefly review the triple Regge formalism, which is essential to describe inclusive polarized proton-proton collision with the pion production. In Sec. III, we show how the TSSA can be derived, based on the triple Regge formalism. In Sec. IV, we demonstrate that triple Regge exchange explains successfully the RHICf experimental data on TSSA. We then discuss the significance of the interference effects between triple Regge diagrams. Section V summarizes the present work and draw conclusions.

*heejin.kim@inha.edu
†sclymton@inha.edu
‡hchkim@inha.ac.kr

II. TRIPLE REGGE EXCHANGE

The applications of the Regge approach to inclusive hadronic reactions is dated back to the 1970s [26–32]. Mueller generalized the optical theorem for inclusive reactions: The differential cross section for the two-body inclusive reaction, $a + b \to c + X$, can be written in terms of discontinuity of the three-body process $ab\bar{c} \to ab\bar{c}$ along the missing mass $M_X^2 = (p_a + p_b - p_c)^2$. It was shown that the three-body amplitude has the Regge singularities similar to those for the two-body process [26,33]. Triple Regge exchange is obtained from an asymptotic behavior of the Mueller amplitude in the kinematic boundary. It was shown that the unpolarized cross section was successfully described by triple Regge pole contributions [30]. The triple Regge formalism even provides a robust tool for understanding diffractive processes [34–36]. It was anticipated that the nondiagonal triple Regge pole diagram would be able to present the polarization effects [32,37]. However, the statistics of the experiments were very poor, so that no significant data were reported at that time. Only very recently, the RHICf experiment accomplished a measurement of the TSSA in the very forward direction [25].

Since the final particles have very high pseudorapidities and low transverse momenta, one can use Regge exchange of the initial proton as shown in Fig. 1(a). As mentioned previously, the generalized optical theorem leads to Fig. 1(b) with the discontinuity on the complex M_X^2 plane. When M_X^2 is sufficiently large, $ip \to jp$ scattering can be also expressed as a Regge pole. Thus one can consider triple Regge exchange to derive the TSSA as drawn in Fig. 1(c). We extend the formalism in Ref. [32] with baryon Regge trajectories introduced. Note that the spin should be transferred by the baryon Reggeons, since the produced pion does not carry any spin from the polarized proton.

The Lorentz-invariant differential cross section for the inclusive reaction $p + p^h \to \pi^0 + X$ in the high energy limit is given by

$$d\sigma^h \equiv E\frac{d^3\sigma^h}{d^3\boldsymbol{p}} = \frac{1}{s}\sum |A^{\mathrm{tot}}_{p\to\pi^0}(s, p_T; h)|^2, \tag{1}$$

where h represents the helicity direction of the polarized proton beam. s denotes the square of the energy in the center of mass (CM) framework, which is one of the Mandelstam variables. p_T stands for the transverse momentum. When the energy is high enough to apply the Regge formalism, we can employ the generalized optical theorem by Mueller [26] to express $d\sigma^h$ in terms of two Reggeon exchange i and j and the scattering of the unpolarized proton and the Reggeon with the energy M_X^2 as depicted in Fig. 1.

In the limit $M_X^2 \to \infty$, the discontinuity of the $i + p \to j + p$ scattering will follow the Regge behavior as

$$\mathrm{Disc}\, A_{ip\to jp}(M_X^2) = \sum_k G_k^{ij}(t)\gamma_k^{pp}(0)\left(\frac{M_X^2}{s_0}\right)^{\alpha_k(0)}, \tag{2}$$

where $G_k^{ij}(t)$ represents the triple Reggeon coupling given as a function of t that is a square of the momentum transfer (one of the Mandelstam variables), corresponding to the black blob in Fig. 1(c). We will discuss it later. γ_k^{pp} is the vertex function for the ppk vertex in Fig. 1(c). s_0 denotes the scale parameter, which is traditionally given to be around 1 GeV^2. Then $d\sigma^h$ is written as

$$d\sigma^h = \frac{1}{s}\sum_{i,j,k}\sum_{\lambda}\beta^i_{h\lambda}\beta^{j*}_{h\lambda}\mathcal{P}_i\mathcal{P}_j^* G_k^{ij}(t)\gamma_k^{pp}(0)\left(\frac{M_X^2}{s_0}\right)^{\alpha_k(0)}, \tag{3}$$

where $\beta^{i(j)}$ stands for the residue of $i(j)$ exchange. As mentioned previously, the unpolarized proton does not carry any information on its spin to the final state. This implies that k exchange will not affect the spin polarization of particle i, so the helicity of i does not flip:

$$d\sigma^h \sim \sum_{\lambda,\mu}\beta^i_{h\lambda}\beta^{j*}_{h\mu}\delta_{\lambda\mu} \sim \sum_{\lambda}\beta^i_{h\lambda}\beta^{j*}_{h\lambda}. \tag{4}$$

$\mathcal{P}_i(t)$ in Eq. (3) designates the Reggeon propagator [33,38] defined as

$$\mathcal{P}_i(t) \equiv \alpha'_B\xi_i^{\pm}(t)\Gamma(J_i - \alpha_i(t))(1 - x_F)^{-\alpha_i(t)}, \tag{5}$$

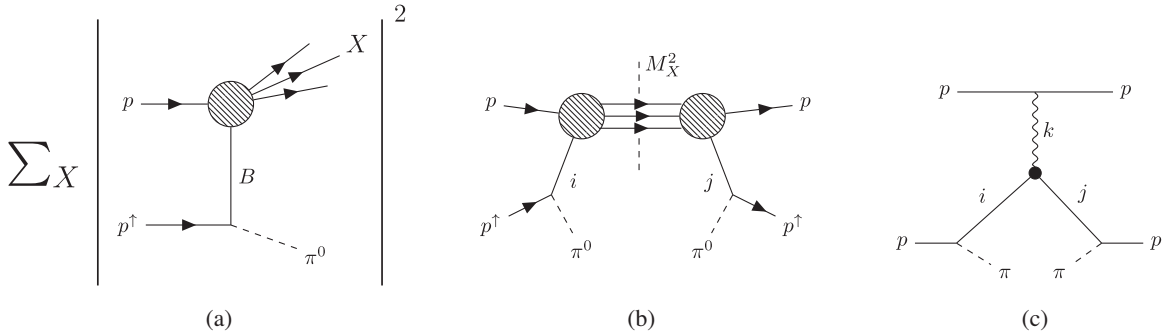

FIG. 1. Diagrammatic representation of $d\sigma^h$ and triple Regge diagram. $d\sigma^h$ is proportional to diagram (a). It can be approximated to (b) in the high energy region. Diagram (c) illustrates that with triple Regge exchange. When M_X^2 is large, (b) can be replaced by (c).

where $\alpha_i(t)$ and J_i denote, respectively, the Regge trajectory and the spin for particle i. The signature factor is given by

$$\xi_i(t) = \frac{1 + \tau_i \exp\{-i\pi(\alpha_i(t) - 0.5)\}}{2}, \tag{6}$$

where τ_i represents the signature of the corresponding Reggeon, i.e., $\tau_i = (-1)^{J_i - 1/2}$.

We introduce the Reggeons corresponding to the proton, the $\Delta(1232)$ isobar, the excited baryon $N^*(1520)$, and the $\Delta(1600)$ isobar with negative parity to derive the TSSA of very forward pion production as depicted in Fig 1. The Regge trajectories for these baryons are given by

$$\begin{aligned} &\alpha_N(t) = -0.35 + 0.99t, \quad && \alpha_{N^*}(t) = -0.73 + 0.95t, \\ &\alpha_\Delta(t) = 0.16 + 0.89t, && \alpha_{\Delta^*}(t) = -0.56 + 0.80t, \end{aligned} \tag{7}$$

which are extracted from the PDG data [39]. Note that the baryonic Regge trajectories contain inevitable uncertainties due to the experimental uncertainties. Since the Regge approach does not provide the vertex structure, we need to employ the effective Lagrangians for the $NN\pi$, $N\Delta\pi$, $NN^*\pi$, and $N\Delta^*\pi$ vertices, given by [40,41]

$$\begin{aligned} \mathcal{L}_{\pi NN} &= -\frac{f_{\pi NN}}{m_\pi}\bar{\psi}\gamma_\mu\gamma_5\boldsymbol{\tau}\cdot\psi\partial^\mu\boldsymbol{\pi}, \\ \mathcal{L}_{\pi NN^*} &= -i\frac{f_{\pi NN^*}}{m_\pi}\bar{\psi}^\mu_{N^*}(g_{\mu\nu} + a\gamma_\mu\gamma_\nu)\gamma_5\boldsymbol{\tau}\cdot\psi\partial^\nu\boldsymbol{\pi}, \\ \mathcal{L}_{\pi N\Delta} &= -\frac{f_{\pi N\Delta}}{m_\pi}\bar{\psi}^\mu_{\Delta}(g_{\mu\nu} + a\gamma_\mu\gamma_\nu)\boldsymbol{T}\cdot\psi\partial^\nu\boldsymbol{\pi}, \\ \mathcal{L}_{\pi N\Delta^*} &= -\frac{f_{\pi N\Delta^*}}{m_\pi}\bar{\psi}^\mu_{\Delta^*}(g_{\mu\nu} + a\gamma_\mu\gamma_\nu)\boldsymbol{T}\cdot\psi\partial^\nu\boldsymbol{\pi}, \end{aligned} \tag{8}$$

where ψ, ψ^μ and π denote, respectively, the Dirac, Rarita-Schwinger, and pseudoscalar fields for the nucleon, Δ isobar, and the pion. $f_{\pi NN}, f_{\pi NN^*}, f_{\pi N\Delta}$, and $f_{\pi N\Delta^*}$ designate the strong coupling constants for the corresponding vertices and m_π is the pion mass. These couplings constants are absorbed into the triple Regge coupling. $\boldsymbol{\tau}$ represents the Pauli matrix for the isospin $1/2$ operator and $\boldsymbol{T}$ stands for the isospin transition operator from isospin $1/2$ to $3/2$ states. $g_{\mu\nu}$ is the metric tensor $g_{\mu\nu} = \mathrm{diag}(1, -1, -1, -1)$ and a the off-shell parameter for the spin $3/2$ baryon.

The Regge factorization implies that the Born amplitudes for one-particle exchange (OPE) can be subdivided into residues for each vertex and Reggeon propagator. The proton-baryon-pion vertex functions are computed from the given effective Lagrangian, respectively, as follows:

$$\begin{aligned} \beta^N_{\lambda\lambda'}(p_T) &= \bar{u}_N(\lambda', q)\not{k}\gamma_5 u_p(\lambda, p), \\ \beta^{N^*}_{\lambda\lambda'}(p_T) &= i\bar{u}^\mu_{N^*}(\lambda', q)(k_\mu + a\gamma_\mu\not{k})\gamma_5 u_p(\lambda, p)), \\ \beta^{\Delta}_{\lambda\lambda'}(p_T) &= \bar{u}^\mu_{\Delta}(\lambda', q)(k_\mu + a\gamma_\mu\not{k})u_p(\lambda, p), \\ \beta^{\Delta^*}_{\lambda\lambda'}(p_T) &= \bar{u}^\mu_{\Delta^*}(\lambda', q)(k_\mu + a\gamma_\mu\not{k})u_p(\lambda, p), \end{aligned} \tag{9}$$

where p, k, and q are the four-momenta of the proton, pion, and the exchanged Reggeon. $u(\lambda)$ and $u^\mu(\lambda)$ denote the Dirac and Rarita-Schwinger spinors for the spin-$1/2$ and spin-$3/2$ baryons, respectively. For simplicity, we will switch off the off-shell parameter a in Eq. (8) and (9). Note that $\beta^i_{\lambda\lambda'}$ should be real-valued functions, so the signature factor determines the phase of $d\sigma$. It plays a crucial role in deriving the TSSA because of the interference between the triple Regge diagrams.

III. TRANSVERSE SINGLE-SPIN ASYMMETRY

The transverse single spin asymmetry is defined by the ratio of the spin-dependent and spin-average differential cross sections:

$$A_N = \frac{d\Delta\sigma_\perp}{d\sigma} = \frac{d\sigma^\uparrow - d\sigma^\downarrow}{d\sigma^\uparrow + d\sigma^\downarrow}, \tag{10}$$

where $\uparrow(\downarrow)$ indicates the polarization of the proton in the transverse direction. Inserting Eq. (1) into Eq. (10), we can straightforwardly compute A_N.

Before we derive the explicit expression for A_N, we discuss the parity invariance of β^i that will provide two constraints. Firstly, $d\sigma$ vanishes if state k has unnatural parity. A matrix element that consists of two fermions (1, 2) and a spinless particle (3) obeys the following parity relation $\beta^3_{\lambda_1\lambda_2} = \eta_1\eta_2\eta_3(-)^{\lambda_1-\lambda_2}\beta^3_{-\lambda_1,-\lambda_2}$, where η_i denotes the naturality of a particle i determined by multiplying the signature and parity quantum number, i.e., $\eta_i = \tau_i P$ [42]. Since the proton has natural parity, we obtain $\eta_1\eta_2 = +1$. So, the residue of the ppk vertex satisfies the parity relation $\beta^k_{\lambda\mu} = \eta_k(-)^{\lambda-\mu}\beta^k_{-\lambda,-\mu}$. It leads to $\gamma^{pp}_k(0) = \sum_\nu \beta^k_{\nu\nu} = (1 + \eta_k)\beta^k_{++}$, which becomes zero when state k has unnatural parity. For example, the following particles such as π, a_1, etc. have unnatural parity. Thus only the particles with natural parity, $k = \mathbb{P}, \rho, \omega, a_2$, etc., can contribute to A_N. Here $\mathbb{P}$ represents the Pomeron. Following Eq. (3), we find that Pomeron exchange contributes to $d\sigma^h$ dominantly over other meson exchanges that have $\alpha_k(0)$ less than 0.5. Secondly, $d\Delta\sigma_\perp$ vanishes when i and j have opposite naturality to each other. Since the transversely polarized state is expressed in terms of positive and negative helicity states quantized along the z-axis: $|\uparrow\rangle = (|+\rangle + i|-\rangle)/\sqrt{2}$ and $|\downarrow\rangle = (|+\rangle - i|-\rangle)/\sqrt{2}$, the residue functions in Eq. (3) are expressed as

$$\beta^i_{\uparrow\lambda} = \frac{1}{\sqrt{2}}(\beta^i_{+\lambda} + i\beta^i_{-\lambda}), \qquad \beta^i_{\downarrow\lambda} = \frac{1}{\sqrt{2}}(\beta^i_{+\lambda} - i\beta^i_{-\lambda}). \tag{11}$$

Using the fact that $\eta_p = +1$ and $\eta_\pi = -1$, we observe

$$d\Delta\sigma_\perp \sim \sum_{\lambda=-1/2}^{1/2} (\beta^i_{+\lambda}\beta^j_{-\lambda} - \beta^i_{-\lambda}\beta^j_{+\lambda}) = (1+\eta_i\eta_j)\beta^i_{+\lambda}\beta^j_{-\lambda}. \quad (12)$$

Thus $d\Delta\sigma_\perp$ vanishes when $\eta_i\eta_j = -1$. The spin-dependent differential cross-section with Pomeron exchange is written as sum of natural and unnatural parity states

$$d\Delta\sigma_\perp = d\Delta\sigma^N_\perp + d\Delta\sigma^U_\perp. \quad (13)$$

Among the particles with the natural parity, the most dominant trajectory with natural parity is the proton one. The next one is the excited nucleon $N^*(1520)$ of which the spin-parity quantum numbers are given by $J^P = 3/2^-$:

$$d\Delta\sigma^N_\perp = \frac{1}{s}\sum_\lambda \beta^N_{+\lambda}\beta^{N^*}_{-\lambda} 2\mathrm{Im}\mathcal{P}_N\mathcal{P}^*_{N^*} \times \sum_k G^{NN^*}_k(t)\gamma^{pp}_k(0)\left(\frac{M_X^2}{s_0}\right)^{\alpha_k(0)}. \quad (14)$$

As for the unnatural parity states, the interference between Δ and $\Delta(1600)$ exchanges furnishes the most dominant contribution:

$$d\Delta\sigma^U_\perp = \frac{1}{s}\sum_\lambda (\beta^\Delta_{+\lambda}\beta^{\Delta^*}_{-\lambda}) 2\mathrm{Im}\mathcal{P}_\Delta\mathcal{P}^*_{\Delta^*} \times \sum_k G^{\Delta\Delta^*}_k(t)\gamma^{pp}_k(0)\left(\frac{M_X^2}{s_0}\right)^{\alpha_k(0)}. \quad (15)$$

On the other hand, the diagonal terms with the leading trajectories substantially contribute to the spin-averaged differential cross section. We also take into account the interferences ($i \neq j$), since those terms are necessary to describe the experimental data:

TABLE I. Numerical values of the parameters $g^{ij}_{\mathbb{P}}$ and $b^{ij}_{\mathbb{P}}$. The first column lists the values of $g^{ij}_{\mathbb{P}}$ with i and j given whereas the second column shows the values of $b^{ij}_{\mathbb{P}}$.

	$g^{ij}_{\mathbb{P}}$	$b^{ij}_{\mathbb{P}}[\mathrm{GeV}^{-2}]$
NN^*	0.028	0.2
$\Delta\Delta^*$	−0.018	0
N^*N^*	0.10	0
$\Delta\Delta$	0.022	0
$\Delta^*\Delta^*$	0.079	0

$$d\sigma = \frac{1}{s}\sum_\lambda \left[\sum_i 2(\beta^i_{+\lambda})^2|\mathcal{P}^2_i|G^{ii}_{\mathbb{P}}(t) + \sum_{i\neq j}\beta^i_{+\lambda}\beta^j_{+\lambda} 2\mathrm{Re}\mathcal{P}_i\mathcal{P}^*_j G^{ij}_{\mathbb{P}}(t)\right] \times \gamma^{pp}_{\mathbb{P}}(0)\left(\frac{M_X^2}{s_0}\right)^{\alpha_{\mathbb{P}}(0)}. \quad (16)$$

The triple Regge coupling $G^{ij}_{\mathbb{P}}(t)$ is often parametrized as $G(t) = G(0)e^{bt}$, because it can not be theoretically determined. In the present work, we parametrize the form of the triple Regge couplings so that we can describe the RHICf data: $G^{ii}_{\mathbb{P}}(t) = G^{ii}_{\mathbb{P}}(0)e^{-B^{ii}_{\mathbb{P}}|t|}$, $G^{ij}_{\mathbb{P}}(t) = G^{ij}_{\mathbb{P}}(0)\sqrt{|t|}e^{-B^{ij}_{\mathbb{P}}|t|}/m_\pi$. We define the following parameters:

$$g^{ij}_{\mathbb{P}} \equiv G^{ij}_{\mathbb{P}}(0)/G^{NN}_{\mathbb{P}}(0), \qquad b^{ij}_{\mathbb{P}} \equiv B^{ij}_{\mathbb{P}} - B^{NN}_{\mathbb{P}} \quad (17)$$

and fit them to the RHICf data. In Table I, we list the numerical values of $g^{ij}_{\mathbb{P}}$ and $b^{ij}_{\mathbb{P}}$. Note that $b^{ij}_{\mathbb{P}}$ comes from the subtraction given by Eq. (13). Except for the $\mathbb{P}NN^*$ vertex, all the values of $b^{ij}_{\mathbb{P}}$ are set to be zero to minimize theoretical uncertainties. Finally, inserting Eqs. (14)–(16) into Eq. (10), we arrive at the expression for the transverse single-spin asymmetry:

$$A_N = \frac{\sum_\lambda[\beta^N_{+\lambda}\beta^{N^*}_{-\lambda}\mathrm{Im}\mathcal{P}_N\mathcal{P}^*_{N^*}(\sqrt{|t|}/m_\pi)g^{NN^*}_{\mathbb{P}} + \beta^\Delta_{+\lambda}\beta^{\Delta^*}_{-\lambda}\mathrm{Im}\mathcal{P}_\Delta\mathcal{P}^*_{\Delta^*}(\sqrt{|t|}/m_\pi)g^{\Delta\Delta^*}_{\mathbb{P}}e^{-b^{\Delta\Delta^*}_{\mathbb{P}}|t|}]}{\sum_\lambda[\sum_i(\beta^i_{+\lambda})^2|\mathcal{P}^2_i|g^{ii}_{\mathbb{P}}e^{-b^{ii}_{\mathbb{P}}|t|} + \sum_{i\neq j}\beta^i_{+\lambda}\beta^j_{+\lambda}\mathrm{Re}\mathcal{P}_i\mathcal{P}^*_j(\sqrt{|t|}/m_\pi)g^{ij}_{\mathbb{P}}e^{-b^{ij}_{\mathbb{P}}|t|}]}. \quad (18)$$

IV. RESULTS AND DISCUSSION

The RHICf Collaboration has first measured A_N for $p + p^\uparrow \to \pi + X$ as a function of p_T with several different ranges of x_F given. In accordance with the Abarbanel-Gross theorem where the triple Regge exchange does not yield the A_N in the backward direction [28], the backward TSSA in RHICf experiment are almost consistent with zero [25]. We thus concentrate on A_N with positive values of x_F.

In Fig. 2 we show the numerical results for A_N given as a function of the transverse momenta p_T with four different ranges of x_F, compared with the RHICf data [25]. The present results are in quantitative agreement with the data. The value of A_N starts to increase as p_T increases till p_T reaches 0.2–0.3 GeV/c. Then, it seems saturated for a while and enlarges again as p_T further increases. Note that in general the experimental uncertainties become larger as p_T increases.

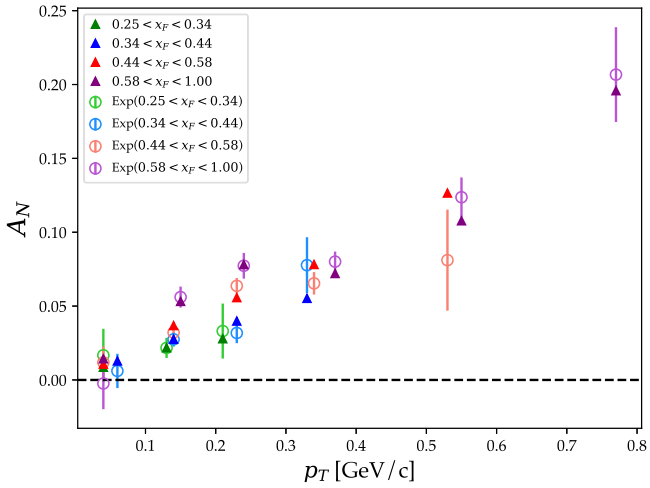

FIG. 2. Numerical results for the TSSA as a function of p_T with several ranges of x_F given. The present results are depicted by the triangles. The open circles with error bars illustrate the RHICf data [25].

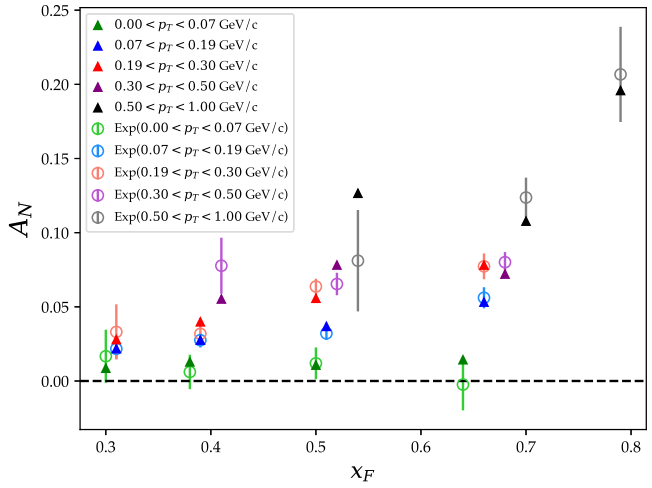

FIG. 3. The TSSA as a function of x_F with several ranges of p_T given. Notations are the same as in Fig. 2.

Figure 3 displays the numerical results for A_N as a function of x_F with five different ranges of p_T given [25]. The current results exhibit an outstanding fit with the RHICf data, in particular, as p_T becomes smaller. Note that when p_T approaches zero, A_N is suppressed.

To scrutinize the current results, we plot A_N as a function of p_T and x_F in Fig. 4. One can see the curve where the A_N equals to zero due to $\sqrt{|t|} = 0$ in the triple Regge coupling. In the region where p_T is lower than this curve, NN^* term governs the TSSA, especially for small x_F. As for the higher p_T, NN^* contributions have negative values. Large and positive $\Delta\Delta^*$ term compensates it, so the total A_N becomes positive. In addition, the pole contributions NN and N^*N^* gradually decrease as x_F increases. N^*N^* term is

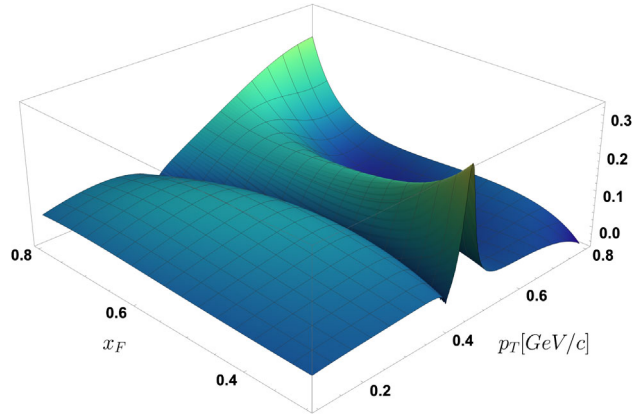

FIG. 4. The 3d plot of A_N as a function of p_T and x_F.

almost consistent with zero for $p_T > 0.8$ GeV/c. Here $\Delta^*\Delta^*$ contribution comes into play to moderate A_N. It is notable to see the peak in the mid-p_T range (~0.5 GeV/c), in particular, when x_F is small. We can understand this feature of A_N by examining the characteristics of the signature factor. At certain values of p_T and x_F, A_N becomes very sensitive to signature factor of the proton. The peak structure of A_N occurs because of this sensitivity. On the other hand, when x_F is large, the diagonal terms such as NN, N^*N^*, $\Delta\Delta$, and $\Delta^*\Delta^*$ diagrams come into play, the peak structure gets smeared. As x_F becomes very small ($x_F < 0.3$), all the signature factors bring about a rapid oscillation of A_N. It indicates that the current scheme of the triple Regge exchange breaks down when x_F is very small.

V. SUMMARY AND CONCLUSIONS

In this work, we aimed at investigating the transverse single spin asymmetries for the neutral pion production from inclusive polarized proton and proton collision, emphasizing the triple Regge exchange that consists of two baryons and a Pomeron. The numerical results of the current work are in quantitative agreement with the RHICf data. We discussed the feature of the transverse single spin asymmetries with p_T and x_F varied. When the pseudorapidity is large and x_F is not very small, we can interpret the neutral pion production from inclusive polarized proton and proton collision as a diffractive one.

ACKNOWLEDGMENTS

The authors are grateful to M. H. Kim and B. Hong at the Center for Extreme Nuclear Matters, Korea University. The present work was supported by Basic Science Research Program through the National Research Foundation of Korea funded by the Ministry of Education, Science and Technology (Grants No. 2021R1A2C2093368 and No. 2018R1A5A1025563).

[1] J. Ashman *et al.* (European Muon Collaboration), Phys. Lett. B **206**, 364 (1988).
[2] X. D. Ji, Phys. Rev. Lett. **78**, 610 (1997).
[3] J. Adam *et al.*, Electron-Ion Collider at Brookhaven National Laboratory: Conceptual Design Report, edited by J. Beebe-Wang (2021).
[4] A. Accardi, J. L. Albacete, M. Anselmino, N. Armesto, E. C. Aschenauer, A. Bacchetta, D. Boer, W. K. Brooks, T. Burton, and N. B. Chang *et al.*, Eur. Phys. J. A **52**, 268 (2016).
[5] M. Anselmino, A. Mukherjee, and A. Vossen, Prog. Part. Nucl. Phys. **114**, 103806 (2020).
[6] R. D. Klem, J. E. Bowers, H. W. Courant, H. Kagan, M. L. Marshak, E. A. Peterson, K. Ruddick, W. H. Dragoset, and J. B. Roberts, Phys. Rev. Lett. **36**, 929 (1976).
[7] D. L. Adams *et al.* (E581 and E704 Collaborations), Phys. Lett. B **261**, 201 (1991).
[8] B. I. Abelev *et al.* (STAR Collaboration), Phys. Rev. Lett. **101**, 222001 (2008).
[9] A. Adare *et al.* (PHENIX Collaboration), Phys. Rev. D **90**, 012006 (2014).
[10] U. A. Acharya *et al.* (PHENIX Collaboration), Phys. Rev. D **103**, 052009 (2021).
[11] J. Adam *et al.* (STAR Collaboration), Phys. Rev. D **103**, 092009 (2021).
[12] E. C. Aschenauer, C. Aidala, A. Bazilevsky, M. Diehl, R. Fatemi, C. Gagliardi, Z. Kang, Y. V. Kovchegov, J. Jalilian-Marian, and J. Lajoie *et al.*, arXiv:1602.03922.
[13] D. W. Sivers, Phys. Rev. D **41**, 83 (1990).
[14] J. C. Collins, Nucl. Phys. **B396**, 161 (1993).
[15] J. C. Collins, S. F. Heppelmann, and G. A. Ladinsky, Nucl. Phys. **B420**, 565 (1994).
[16] A. V. Efremov and O. V. Teryaev, Sov. J. Nucl. Phys. **36**, 140 (1982).
[17] H. Eguchi, Y. Koike, and K. Tanaka, Nucl. Phys. **B763**, 198 (2007).
[18] J. w. Qiu and G. F. Sterman, Nucl. Phys. **B378**, 52 (1992).
[19] J. w. Qiu and G. F. Sterman, Phys. Rev. Lett. **67**, 2264 (1991).
[20] L. Gamberg, Z. B. Kang, and A. Prokudin, Phys. Rev. Lett. **110**, 232301 (2013).
[21] K. Kanazawa, Y. Koike, A. Metz, and D. Pitonyak, Phys. Rev. D **89**, 111501 (2014).
[22] L. Gamberg, Z. B. Kang, D. Pitonyak, and A. Prokudin, Phys. Lett. B **770**, 242 (2017).
[23] L. Gamberg, M. Malda, J. A. Miller, D. Pitonyak, A. Prokudin, and N. Sato, Phys. Rev. D **106**, 034014 (2022).
[24] J. Cammarota, L. Gamberg, Z.-B. Kang, J. A. Miller, D. Pitonyak, A. Prokudin, T. C. Rogers, and N. Sato (Jefferson Lab Angular Momentum Collaboration), Phys. Rev. D **102**, 054002 (2020).
[25] M. H. Kim *et al.* (RHIC-f Collaboration), Phys. Rev. Lett. **124**, 252501 (2020).
[26] A. H. Mueller, Phys. Rev. D **2**, 2963 (1970).
[27] A. H. Mueller, Phys. Rev. D **4**, 150 (1971).
[28] H. D. I. Abarbanel and D. J. Gross, Phys. Rev. Lett. **26**, 732 (1971).
[29] R. J. N. Phillips, G. A. Ringland, and R. P. Worden, Phys. Lett. **40B**, 239 (1972).
[30] R. D. Field and G. C. Fox, Nucl. Phys. **B80**, 367 (1974).
[31] S. Y. Chu, B. R. Desai, B. C. Shen, and R. D. Field, Phys. Rev. D **13**, 2967 (1976).
[32] F. E. Paige and D. P. Sidhu, Phys. Rev. D **14**, 2307 (1976).
[33] P. D. B. Collins *An Introduction to Regge Theory and High Energy Physics* (Cambridge University Press, Cambridge, England, 1977).
[34] R. Fiore, A. Flachi, L. L. Jenkovszky, F. Paccanoni, and A. Papa, Phys. Rev. D **61**, 034004 (2000).
[35] A. A. Godizov, Nucl. Phys. **A955**, 228 (2016).
[36] E. Levin and M. Siddikov, Eur. Phys. J. C **79**, 376 (2019).
[37] R. D. Field, Polarization effects in inclusive processes. 2, Report No. CALT-68-459 (1974).
[38] A. Donnachie, H. G. Dosch, P. V. Landshoff, and O. Nachtmann *Pomeron Physics and QCD* (Cambridge University Press, Cambridge, England, 2002).
[39] R. L. Workman *et al.* (Particle Data Group), Prog. Theor. Exp. Phys. **2022**, 083C01 (2022).
[40] R. Machleidt, K. Holinde, and C. Elster, Phys. Rep. **149**, 1 (1987).
[41] V. Pascalutsa and O. Scholten, Nucl. Phys. **A591**, 658 (1995).
[42] J. K. Storrow, Phys. Rep. **103**, 317 (1984).